Applied Physics B (2021) 127:167
https://doi.org/10.1007/s00340-021-07715-5

Applied Physics B
Lasers and Optics

Polarization-entangled biphoton states: a comparison of biperiod waveguides in KTP and LN

Vineet Kumar Shukla[1] · **Joyee Ghosh**[1]

Received: 10 July 2021 / Accepted: 4 November 2021 / Published online: 20 November 2021

Abstract
In this paper, we study the generation of polarization-entangled biphoton states in $\chi^{(2)}$ waveguides through spontaneous parametric downconversion, based on type-0, type-I and type-II quasi-phase-matching. The response of two popular nonlinear crystals: potassium titanyl phosphate (KTP) and lithium niobate (LN) are compared. An analysis of the joint spectral amplitude ensures which parameters are ambient for generating frequency-correlated photons in the phase-matching spectrum of each material. We have studied three examples of different pump wavelengths, with the signal photon being emitted at the telecommunication wavelength of 1550 nm in each case. Polarization-entangled photon pairs are produced in the $|\psi^+\rangle$, or $|\phi^+\rangle$ state, utilizing dual quasi-phase-matching conditions in each case. Both these cases are analyzed separately and compared for KTP and LN. We also compare the efficient generation of maximally entangled photon pairs by calculating the von Neumann entropy in these cases.

1 Introduction

Entangled photons are necessary building blocks for quantum information processing, such as quantum key distribution, quantum teleportation, superdense coding, quantum networks, and quantum computing [1]. In almost all quantum communication systems, a powerful resource for transmitting data through channels or free space is accomplished by entangled photons. They have been generated through a few techniques, most efficiently using spontaneous parametric downconversion (SPDC) [2] utilizing the second-order nonlinearity in crystals. In a recent review [3] on SPDC sources, bulk nonlinear materials with cw pump are compared to waveguide-based sources in integrated platforms. Polarization-entangled photon sources in different phase-matching geometries are covered as well as the progress of entangled photon sources in other degrees of freedom are well discussed. The physics and technology of generating and manipulating entangled photons in guided-wave nonlinear crystals with appreciable second-order nonlinearities such as potassium titanyl phosphate (KTP) or lithium niobate (LN) have been topics of immense interest [4].

Such integrated waveguides can enable the direct generation of novel and useful photonic quantum states with specified properties. The generation of polarization-entangled telecom photons utilizing a single quasi-phase-matching (QPM) was achieved by fabricating a half-wave plate in the middle of a periodically poled lithium niobate (ppLN) waveguide along its propagation axis [5]. On the other hand, a direct generation of polarization-entangled photons is possible based on dual quasi-phase-matching [6–9], studied for KTP and LN waveguides. High-purity polarization-entangled photon pairs in the telecommunication band have been experimentally generated in a ppLN ridge waveguide device using cascaded poling [10]. Multiple quantum interference effects can also enable the generation of high-performance, degenerate, post-selection free, polarization-entangled photons with a high emission rate and broadband distribution [11]. Based on their joint spectral amplitude, biphoton states from a ppLN ridge waveguide, with the signal photon being at telecom wavelength, can be characterized for the extent and type of their correlations [12, 13].

A recent work describes an efficient way to produce polarization-entangled photon pairs based on the bound state in the continuum (BIC) in a lithium niobate waveguide [14] without periodic poling of the waveguide, possible over a wide spectrum from visible to THz regions, with millimeter-long waveguides. An experimental study [15] addresses a hybrid approach utilizing guided-wave and bulk

✉ Joyee Ghosh
joyee@physics.iitd.ac.in

[1] Department of Physics, Indian Institute of Technology Delhi, New Delhi 110016, India

optics in a deterministic scheme to explore a polarization-entangled photon-pair source, demonstrating high-fidelity (96%) singlet state generation with a brightness ~ 2.9×10^6 pairs/(mode s mW). Another study based on semiconductor Bragg-reflection waveguides [16] uses pulsed state preparation and free-running single-photon detection with low pump powers, resulting in strong photon-pair correlation. Exploring time-bin entangled photon generation, the authors demonstrate a high value of concurrence ~ 88.9% and fidelity ~ 94.2% with a Bell state.

Further, based on such dual-period waveguides in LN and KTP, integrated devices can be possibly fabricated that produce 'hyperentangled' photons, being (simultaneously) entangled in spatial mode and polarization degrees of freedom [17, 18]. A different perspective to describe the full temporal and spatial characterization of polarization-entangled photons through SPDC is presented by the authors [19] using an intensified high-speed optical camera as a new characterization method for the spatial distribution of entangled quantum information. Another recent study [20] of quantum imaging utilizing spatial-polarization hyper-entangled photon pairs is used to remotely reconstruct phase images of complex objects. Information encoded into the polarization degree of the entangled state allows imaging through dynamic phase disorder, even in the presence of strong classical noise, with enhanced spatial resolution compared with classical coherent holographic systems.

In this paper, we address the generation of polarization-entangled photon pairs using a combination of quasi-phase-matching conditions and compared them in periodically poled LN and KTP waveguides. We discuss three sets of different pump wavelengths all emitting the signal photon at a telecommunication wavelength of 1550 nm. We have also compared the joint spectral amplitude ensuring suitable parameters for generating frequency-correlated photons in the phase-matching spectrum. Based on the polarization degree of freedom, such photon pairs can be generated in maximally entangled Bell states,

$$|\psi^+\rangle = \frac{1}{\sqrt{2}}\{||e_s, o_i\rangle, + |o_s, e_i\rangle|\}.$$

$$|\phi^+\rangle = \frac{1}{\sqrt{2}}\{||e_s, e_i\rangle, + |o_s, o_i\rangle|\}.$$

where states $|e\rangle$and $|o\rangle$correspond to extraordinary (e-polarized) and ordinary (o-polarized) polarization states of the photon, and subscript s and i correspond to the signal and idler photons, respectively.

In Sect. 2, we give a brief description of the quantum mechanical analysis for SPDC in a waveguide and the generation of polarization-entangled photon pairs. Part (a) details the strategy to generate a $|\psi^+\rangle$ Bell state while part (b) details the strategy to generate a $|\phi^+\rangle$ Bell state. In Sect. 3, we discuss the signal and idler mode profiles in KTP and LN waveguides of the same dimension. In Sect. 4, we present and compare our numerical results pertaining to a practical waveguide structure in ppKTP and ppLN for the above entangled states, corresponding to a signal wavelength of 1550 nm in each case. The entangled states are characterized through a brief comparison of the von Neumann entropy in LN and KTP. In Sect. 5, we investigated the joint spectral amplitude analysis for the biphoton states in the above cases and compared the same for LN and KTP nonlinear material. Finally, in Sect. 6, we summarize our results and conclude the findings.

2 Quantum mechanical analysis

As shown in Fig. 1a, we consider an integrated nonlinear substrate with two z-cut, x-propagating waveguide regions as Path-I and Path-II, well separated by a large distance such that the fields (from these two paths) do not interact with each other. Since a z-cut and x-propagating nonlinear substrate is considered in an integrated waveguide (crystal) device, the optic axis is along the z-axis, and the eigen polarizations are ordinary wave with y-polarization (o-polarization) as the fundamental TE-like mode and extraordinary wave with z-polarization (e- polarization) as the fundamental TM-like mode. We assume a nonlinear interaction takes place only between the fundamental guided modes of a particular waveguide region. Both paths are appropriately and

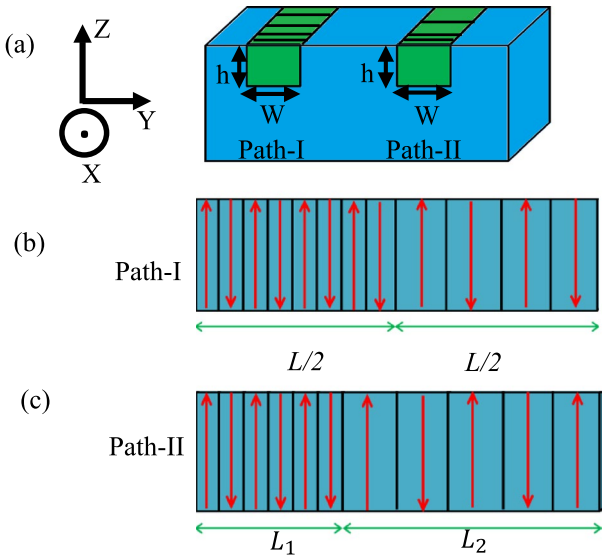

Fig. 1 **a** Waveguide cross-section (front view) with dimensions: $h = W = 6$ µm, and length, $L = 4$ cm (not to scale). Schematic of bipeiod poling profile in waveguide (side view) to achieve: **b** $|\psi^+\rangle$ state of total length L and poling periods $\bigwedge_{eo}$ and $\bigwedge_{oe}$, and **c** $|\phi^+\rangle$ state of total length $L = L^1 + L^2$ and poling periods $\bigwedge_{ee}$ and $\bigwedge_{oo}$, respectively

biperiodically poled to satisfy two separate QPM conditions in each case, required for the generation of a $|\psi^+\rangle$ biphoton state (in Path-I, shown in Fig. 1b), and a $|\phi^+\rangle$ biphoton state (in Path-II, shown in Fig. 1c), achieved through spontaneous parametric downconversion.

(a) $|\psi^+\rangle$ state (in Path-I)

We consider Path-I with poling periods $\bigwedge_{eo}$ and $\bigwedge_{oe}$, as shown in Fig. 1b, corresponding to two distinct SPDC processes, across equal lengths of $L/2$. The input pump is o-polarized (along y-axis). $\bigwedge_{eo}$ leads to a process that generate an e-polarized signal along with an o-polarized idler, while, $\bigwedge_{oe}$ leads to a process that generate an o-polarized signal and e-polarized idler. Both processes pertain to the d_{24} coefficient of the nonlinear d-tensor. The details of the following phase-matching conditions are given in Ref. [6]. For the generation of SPDC photons starting from a pump photon, the process can be explained through an appropriate interaction Hamiltonian and by evaluating the Schrödinger equation. The pump power is a non-depleted classical field (E_{po}), while signal and idler fields are represented by quantum operators. The electric field distribution for the pump, signal and idler modes in the above scenario are given by

$$\vec{E}_{po} = \frac{1}{2} e_{po}(\vec{r}) E_{po}\left(e^{i(\beta_{po}x-\omega_p t)} + c.c.\right)\hat{y} \tag{1}$$

$$\hat{E}_{so} = i\int d\omega_s e_{so}(\vec{r})\sqrt{\frac{\hbar\omega_s}{\varepsilon_{so}L}}\left(\hat{a}_{so}e^{i\beta_{so}x} + h.c.\right)\hat{y} \tag{2}$$

$$\hat{E}_{se} = i\int d\omega_s e_{se}(\vec{r})\sqrt{\frac{\hbar\omega_s}{\varepsilon_{se}L}}\left(\hat{a}_{se}e^{i\beta_{se}x} + h.c.\right)\hat{z} \tag{3}$$

$$\hat{E}_{io} = i\int d\omega_i e_{io}(\vec{r})\sqrt{\frac{\hbar\omega_i}{\varepsilon_{io}L}}\left(\hat{a}_{io}e^{i\beta_{io}x} + h.c.\right)\hat{y} \tag{4}$$

$$\hat{E}_{ie} = i\int d\omega_i e_{ie}(\vec{r})\sqrt{\frac{\hbar\omega_i}{\varepsilon_{ie}L}}\left(\hat{a}_{ie}e^{i\beta_{ie}x} + h.c.\right)\hat{z} \tag{5}$$

Here, first subscripts p, s and i correspond to pump, signal and idler and second subscripts o and e correspond to o-polarized and e-polarized, respectively. Here, y- and z-directions are treated as the direction of o- and e-polarizations, respectively. The interaction Hamiltonian is

$$\hat{H}_{\text{int}} = -4\varepsilon_0 \iiint d_{24}\vec{E}_{po}\left(\hat{E}_{se}\hat{E}_{io}e^{i\varphi_1} + \hat{E}_{so}\hat{E}_{ie}\right)dxdydz \tag{6}$$

where φ_1 is a constant phase difference picked up by eo-polarized photons, produced in the first region (of length $L/2$) and propagating through the second region (also of length $L/2$) in the biperiod waveguide. Using Eqs. (1, 2, 3, 4, 5), the interaction Hamiltonian is derived as

$$\hat{H}_{\text{int}} = \iint d\omega_s d\omega_i\left\{C_{eo}^{(1)}\left(\hat{a}_{se}^{\dagger}\hat{a}_{io}^{\dagger} + h.c.\right) + C_{oe}^{(1)}\left(\hat{a}_{se}^{\dagger}\hat{a}_{io}^{\dagger} + h.c.\right)\right\} \tag{7}$$

The interaction Hamiltonian operates on the two-photon vacuum state$|0,0\rangle$, found as

$$|\psi(t)\rangle e^{-i\hat{H}_{\text{int}}t/\hbar}|0,0 \tag{8}$$

The output state is

$$|\psi^+\rangle = i\int d\omega_s\left[C_{eo}|e_s,o_i\rangle + C_{oe}|o_s,e_i\rangle\right] \tag{9}$$

where C_{eo} and C_{oe} depend on the ω_s (and ω_i) through the sinc functions, the output state is entangled in the region of their overlap.

The relative values of C_{eo} and C_{oe} will determine whether the output state is maximally entangled [6]. These are related to the overlap integrals and effective indices of the interacting modes at the pump, signal, and idler wavelengths.

(b) $|\phi^+\rangle$ state (in Path-II)

We consider Path-II with poling periods $\bigwedge_{ee}$ and $\bigwedge_{oo}$, with unequal lengths L_1 and L_2, respectively, as shown in Fig. 1c, corresponding to two distinct SPDC processes. The input pump is e-polarized (along z-axis) for this state. $\bigwedge_{ee}$ leads to a process that generate both e-polarized signal and idler photons in length L_1 (pertaining to the d_{33} coefficient), while $\bigwedge_{oo}$ leads to a process that generate both o-polarized signal and idler photons in length L_2 (pertaining to the d_{32} coefficient). The interaction Hamiltonian is given by

$$\hat{H}_{\text{int}} = -4\varepsilon_0 \iiint \left(d_{33}E_{pe}E_{se}E_{ie}e^{i\varphi_2} + d_{32}E_{pe}E_{so}E_{io}\right)dxdydz \tag{10}$$

where $\varphi_2$is a constant phase difference picked up by ee-polarized photons (produced in the region of length L_1), propagating through length L_2 in the periodically poled waveguide. After simplification, the interaction Hamiltonian is derived as

$$\hat{H}_{int} = \iint d\omega_s d\omega_i\left\{C_{ee}^{(1)}\left(\hat{a}_{se}^{\dagger}\hat{a}_{ie}^{\dagger} + h.c.\right) + C_{oo}^{(1)}\left(\hat{a}_{so}^{\dagger}\hat{a}_{io}^{\dagger} + h.c.\right)\right\} \tag{11}$$

The output state is

$$|\phi^+\rangle = i \int d\omega_s \left[C_{ee} |e_s, e_i\rangle + C_{oo} |o_s, o_e\rangle \right] \tag{12}$$

Since C_{oo} and C_{ee} depend on the ω_s (and ω_i) through the sinc functions, the output state is entangled in the region of their overlap. As we have mentioned earlier, the relative values of C_{oo} and C_{ee} will determine if the output state is maximally entangled or not. These are related to the overlap integrals, the effective indices of the interacting modes at the pump, signal and idler wavelength, and the nonlinear d-coefficients for the above two processes along with their respective interaction lengths in the waveguide.

3 Relative modes of the waveguide

In this section, we have computed relative waveguide modes of the signal and idler fields for two different materials, KTP and LN, considering the waveguide dimensions, $w = h = 6$ µm. The pump, signal and idler wavelengths are taken as 532 nm, 1550 nm, and 810 nm, respectively.

(a) KTP: The relevant Sellmeier Equation for refractive index is given by

$$n = \left(A + \frac{B}{\lambda^2 - C} + \frac{D}{\lambda^2 - E} \right)^{1/2}, \lambda \text{ in µm} \tag{13}$$

where for o-polarized, $A = 3.45018$, $B = 0.04341$, $C = 0.04597$, $D = 16.98825$ and $E = 39.43799$. For e-polarized, $A = 4.59423$, $B = 0.06206$, $C = 0.04763$, $D = 110.80672$, and $E = 86.12171$.

The effective indices of the o-polarized and e-polarized mode at the pump, signal, and idler wavelengths are found to be $n_{po} = 1.792316, n_{pe} = 1.892353 n_{so} = 1.736497, n_{se} = 1.817448, n_{io} = 1.758841$, and $n_{ie} = 1.846784$, respectively [21]. The refractive index differences between the substrate and waveguide core as $\Delta n = 0.01$ [22]. The signal/idler modes in this case are shown in Fig. 2.

(b) LN: we had chosen Ti-in-diffused LN due to the fact that the diffusion of Ti increases the refractive index for both o-polarized and e-polarized, and hence the wavelength dispersion is low. Sellmeier Equation for refractive index of lithium niobate is given by

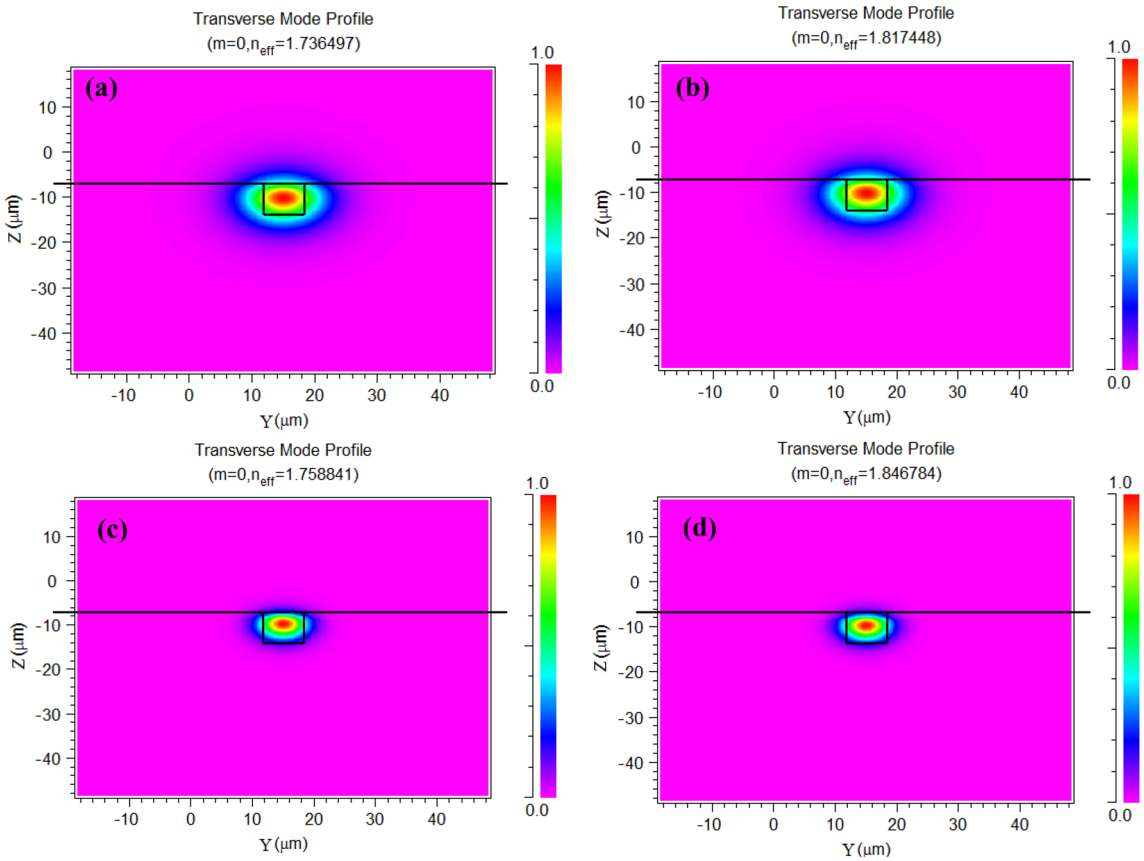

Fig. 2 Field patterns in KTP (of Path-I or Path-II) corresponding to **a** o-polarized signal and **b** e-polarized signal at 1550 nm; **c** o-polarized idler and **d** e-polarized idler at 810 nm

$$n = \left(A + \frac{B}{C + \lambda^2} + D\lambda^2\right)^{1/2}, \lambda \text{ in } \mu m \tag{14}$$

where for o-polarized, $A = 4.9048$, $B = 0.11768$, $C = -0.0475$, and $D = -0.027169$. For e-polarized, $A = 4.582$, $B = 0.099169$, $C = -0.044432$, $D = -0.02195$. Titanium in-diffused channel waveguides is described by the following equation:

$$n^2(y,z) = n_b^2 + 2n_b\Delta n \exp\left(-\frac{y^2}{W^2}\right)\exp\left(-\frac{z^2}{h^2}\right); \quad z < 8$$
$$= n_c^2; \qquad z > 8$$

where n_b is the refractive index of nonlinear material substrate, Δn is the change of the refractive index due to titanium in-diffused, n_c is the refractive of the air, W is the width and h is the height-to-depth of the waveguide.

The following values of various waveguide parameters are $\Delta n_{pe} = 0.0036$, $\Delta n_{po} = 0.0037$, $\Delta n_{so} = \Delta n_{se} = 0.0025$ and $\Delta n_{io} = 0.0033$, $\Delta n_{ie} = 0.0029$ [6, 21]. The effective indices of pump, signal, and idler for o-polarized and e-polarized modes are found to be $n_{po} = 2.324329$, $n_{pe} = 2.234677$, $n_{so} = 2.211199$, $n_{se} = 2.137691$, $n_{io} = 2.254688$, and $n_{ie} = 2.174952$, respectively. The relative signal/idler modes in this case are shown in Fig. 3.

Here, we note, in both KTP and LN, the idler fields are slightly more confined than the signal fields due to their shorter wavelength. A difference in the field patterns leads to a decrease in the overlap integral; however, due to the transverse profile of the fields, the quantities C_{eo} and C_{oe} (with $\Delta K_{eo} = 0$ and $\Delta K_{oe} = 0$) were almost equal, leading to a maximally entangled state.

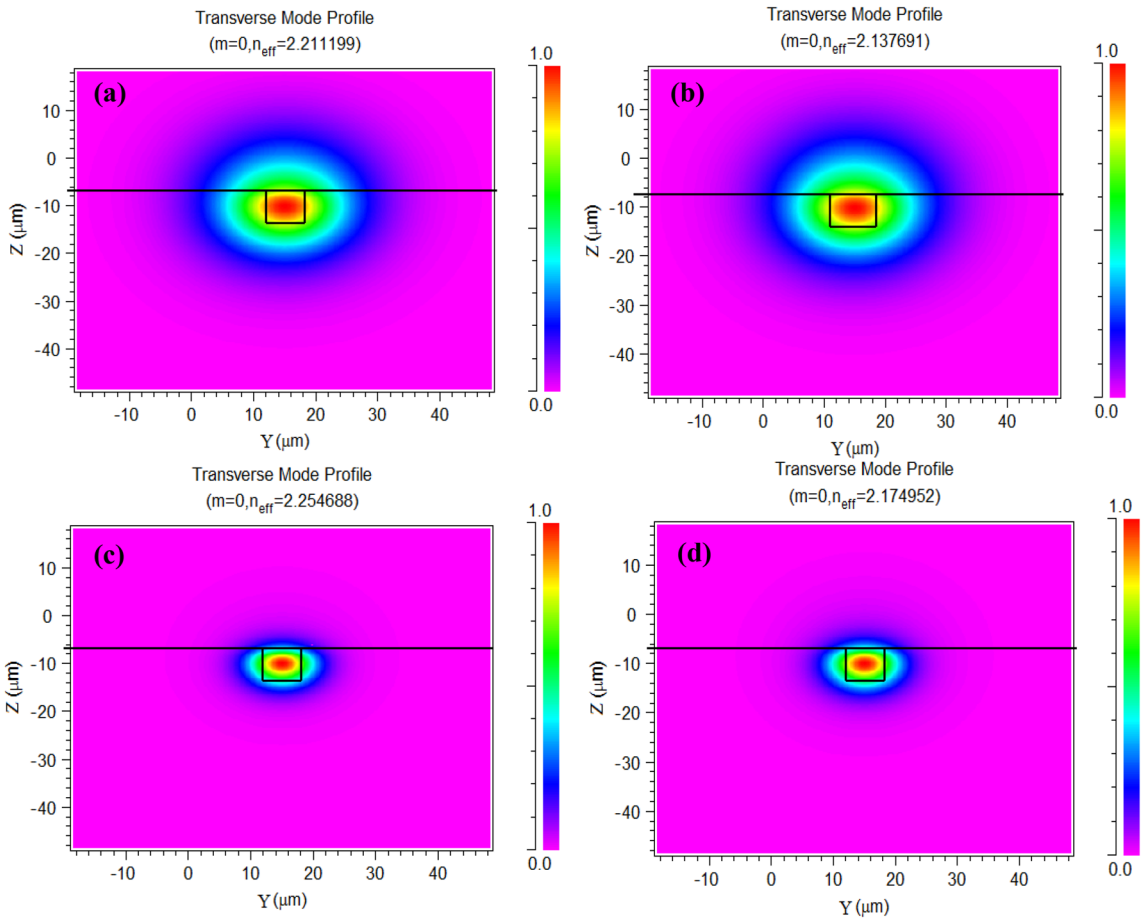

Fig. 3 Field patterns in LN (of Path I or Path II) corresponding to **a** o-polarized signal and **b** e-polarized signal at 1550 nm; **c** o-polarized idler and **d** e-polarized idler at 810 nm

4 Simulation results and discussion

We have simulated three cases of interest based on different pump wavelengths, all emitting the signal photon at the telecommunication wavelength of 1550 nm. In each case, two nonlinear materials, KTP and LN, are compared. They are considered as z-cut crystals with x-propagating fields. The results are detailed in this section for polarization-entangled biphoton states, towards their corresponding Bell's states $|\psi^+\rangle$ and $|\phi^+\rangle$. In all these simulations, the waveguide dimensions are considered as $w = h = 6$ µm while the *total* length of the waveguide is taken as $L = 4$ cm.

(i) Generation of $|\psi^+\rangle$ state

Case–I: $\lambda_p = 532$nm: Here, an o-polarized input pump beam at 532 nm emits a signal at 1550 nm and an idler at 810 nm with orthogonal polarization to the signal, involved in two type-II SPDC processes. In case of a KTP waveguide, the required grating periods for the two downconversion processes corresponding to K_{eo} and K_{oe} spatial frequencies are $\bigwedge_{eo} = 39.91$ µm and $\bigwedge_{oe} = 31.96$ µm, respectively.

Figure 4a(i) shows the calculated bandwidths for the two SPDC processes relevant to the generation of the $|\psi^+\rangle$ Bell state in KTP around the signal wavelength of 1550 nm. The process leading to e-polarized signal and

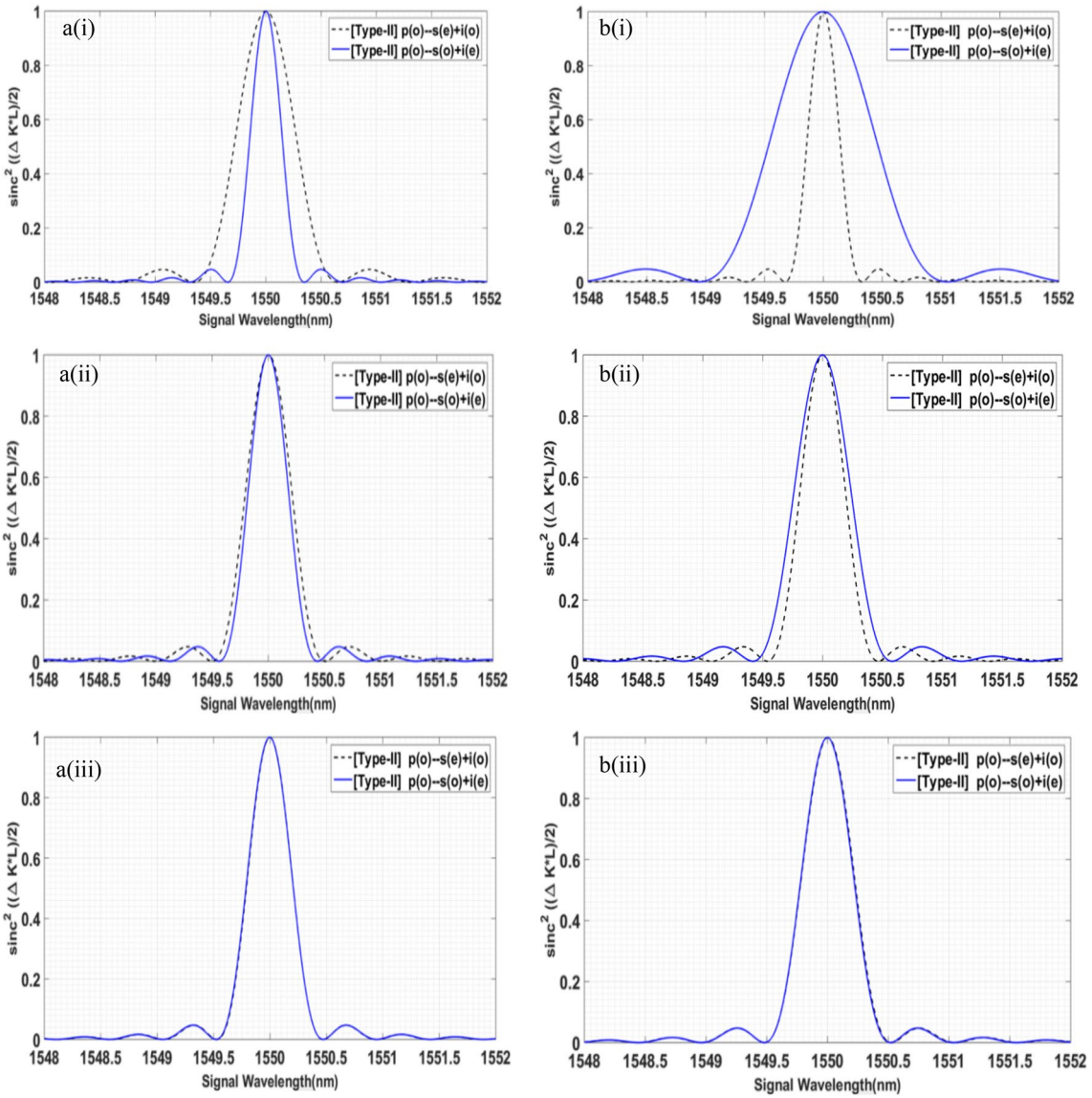

Fig. 4 Calculated bandwidths for two SPDC processes relevant to generation of $|\psi^+\rangle$ state in case of **a** KTP (left-hand panel) and **b** LN (right-hand panel), for a pump wavelength of (i) 532 nm, (ii) 710 nm, and (iii) 777.5 nm. All processes emit the signal around 1550 nm

o-polarized idler gives a bandwidth of 0.58 nm (black dashed curve), while the process leading to *o*-polarized signal and *e*-polarized idler gives a bandwidth of 0.30 nm (blue continuous curve).

In case of LN, the grating periods required, corresponding to K_{eo} and K_{oe} spatial frequencies, are $\bigwedge_{eo} = 4.85\,\mu m$ and $\bigwedge_{oe} = 3.89\,\mu m$, respectively. Figure 4b(i) similarly shows the calculated signal bandwidths for these two processes. The process leading to *e*-polarized signal and *o*-polarized idler gives a bandwidth of 0.29 nm (black dashed curve), while the process leading to *o*-polarized signal and *e*-polarized idler gives a bandwidth of 0.93 nm (blue continuous curve).

Case–II: $\lambda_p = 710nm$: With an (*o*-polarized) input pump at 710 nm, a signal is emitted at 1550 nm and an idler at 1310 nm in type-II SPDC. In KTP, the grating periods are $\bigwedge_{eo} = 40.37\,\mu m$ and $\bigwedge_{oe} = 70.38\,\mu m$ corresponding to K_{eo} and K_{oe} spatial frequencies, respectively. Figure 4a(ii) depicts the calculated signal bandwidths. The process leading to *e*-polarized signal and *o*-polarized idler gives a bandwidth of 0.45 nm (black dashed curve), while the other process gives a bandwidth of 0.39 nm (blue continuous curve).

Similarly, in LN, the required periods are $\bigwedge_{eo} = 8.11.\,\mu m$ and$\bigwedge_{oe} = 7.52\,\mu m$ and Fig. 4b(ii) shows the corresponding bandwidths. The process leading to *e*-polarized signal and *o*-polarized idler gives a bandwidth of 0.41 nm (black dashed curve), while the other process gives a bandwidth of 0.51 nm (blue continuous curve).

Case–III: $\lambda_p = 777.5nm$: Similarly, for a pump at 777.5 nm, a signal at 1550 nm and an idler at 1560 nm are emitted. The relevant QPM grating periods, $\bigwedge_{eo} = 48.59\,\mu m$ and$\bigwedge_{oe} = 49.55\,\mu m$ for the two PDC processes in KTP, with corresponding signal bandwidths shown in Fig. 4a(iii). Both processes (leading to an *e*-polarized signal and an *o*-polarized idler or vice versa) give a bandwidth of ~ 0.42 nm (overlapping black dashed and blue continuous curves) for KTP.

In case of LN, the grating periods are $\bigwedge_{eo} = 9.17\,\mu m$ and $\bigwedge_{oe} = 9.19\,\mu m$ for the two PDC processes, with their signal bandwidths depicted in Fig. 4b(iii). Again, similar to KTP, both processes have a completely overlapping bandwidth of 0.46 nm (black dashed and blue continuous curves).

In all the above cases, irrespective of the nonlinear material, a difference in the bandwidths is noted due to a difference in the signal/idler wavelengths emitted with orthogonal polarizations, in general. Further, in all cases of Fig. 4, the two relevant SPDC processes share a *common* or *overlap* bandwidth relevant to the generation of a $|\psi^+\rangle$ state. These overlap bandwidths, for different input pump wavelengths pertaining to two nonlinear materials, are detailed in Table 1. We observe that the common bandwidth increases as the difference in the signal/idler wavelengths decreases.

Table 1 Common bandwidth for $|\psi^+\rangle$ state, compared for three different input pump wavelengths in two nonlinear materials

S.N	Pump λ_p (nm)	Signal λ_s (nm)	Idler λ_i (nm)	Common bandwidth for $\|\psi^+\rangle$ state (nm)	
				KTP	LN
1	532	1550	810	0.30	0.29
2	710	1550	1310	0.39	0.41
3	777.5	1550	1560	0.42	0.46

Next, we calculate [23] the von Neumann entropy of the polarization-entangled states generated here using

$$S = -\frac{C_{eo}^2}{C_{eo}^2 + C_{oe}^2}\log_2\frac{C_{eo}^2}{C_{eo}^2 + C_{oe}^2} - \frac{C_{oe}^2}{C_{oe}^2 + C_{eo}^2}\log_2\frac{C_{oe}^2}{C_{oe}^2 + C_{eo}^2} \tag{15}$$

To generate a maximally polarization-entangled state defined in Eq. (9), the *C* coefficients should be equal (i.e.$C_{eo} = C_{oe}$). For this, we require $(I_{eo}/n_{se}n_{io} = I_{oe}/n_{so}n_{ie})$, i.e., the corresponding ratio of the overlap integrals and the effective indices of the fields involved should be the same.

Figure 5a, b shows the variation of von Neumann entropy for the two materials, calculated using Eq. (15), as a function of the height of the waveguide for a width of 6μm. As found, the von Neumann entropy for KTP in Fig. 5a is slightly more as compared to that of LN in Fig. 5b, although both are very close to unity, leading to a maximally entangled $|\psi^+\rangle$ state in each case.

(ii) Generation of$|\phi^+\rangle$ state

Case–I: $\lambda_p = 532nm$: Here, an *e*-polarized input pump beam at 532 nm emits a signal at 1550 nm and an idler at 810 nm with same polarizations *ee*- in a type-0 process or *oo*- in a type-I process. In KTP, the grating periods required for these two downconversion processes, corresponding to K_{ee} and K_{oo} spatial frequencies, are $\bigwedge_{ee} = 9.57\,\mu m$ and $\bigwedge_{oo} = 3.77\,\mu m$, respectively.

Figure 6a(i) shows the corresponding calculated signal bandwidths around 1550 nm. The process leading to an *e*-polarized signal and idler gives a bandwidth of 2.68 nm (green continuous curve), while that leading to an *o*-polarized signal and idler gives a bandwidth of 0.96 nm (red dashed curve).

Similarly, in case of LN, the required grating periods are $\bigwedge_{ee} = 7.34\,\mu m$ and $\bigwedge_{oo} = 103.9\,\mu m$, respectively. Figure 6b(i) shows the calculated signal bandwidths in this case. The *e*-polarized signal/idler process has a bandwidth of 6.81 nm (green continuous curve), while the *o*-polarized ones has 0.44 nm (red dashed curve). In both the above

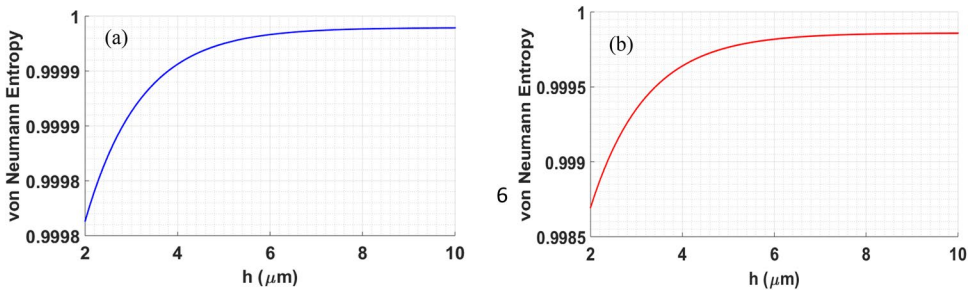

Fig. 5 Variation of von Neumann entropy as a function of the waveguide height (taking width = 6 μm) for the $|\psi^+\rangle$ state in: (a) KTP (blue) and (b) LN (red), corresponding to a pump wavelength of 532 nm

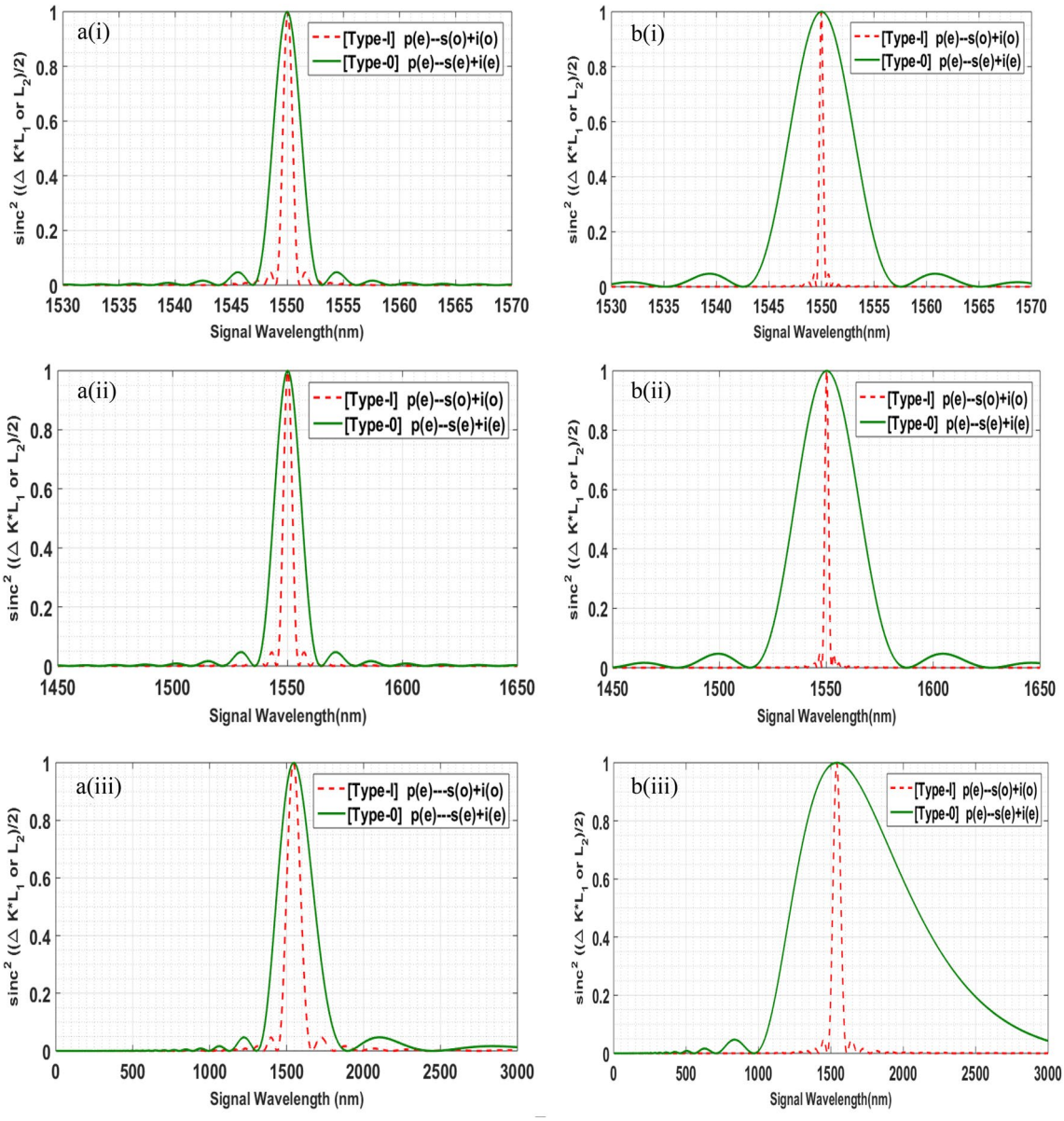

Fig. 6 Calculated bandwidths for two SPDC processes relevant to generation of $|\phi^+\rangle$ state in case of **a** KTP (left-hand panel) and **b** LN (right-hand panel), for a pump wavelength of (i) 532 nm, (ii) 710 nm, and (iii) 777.5 nm. All processes emit the signal around 1550 nm

cases, we observe a huge difference in the emitted bandwidths due to a difference in the types of QPM processes used to generate the $|\phi^+\rangle$ state.

Case–II: $\lambda_p = 710$nm: In KTP, with the input pump at 710 nm, and signal/idler at 1550/1310 nm, the required grating periods are $\bigwedge_{ee} = 19.79\,\mu$m and $\bigwedge_{oo} = 6.04\,\mu$m, for the two SPDC processes, whose calculated signal bandwidths are shown in Fig. 6a(ii). The *ee*- process gives a bandwidth of 12.41 nm (green continuous curve), while the *oo*- process gives 4.40 nm (red dashed curve). Similarly, for LN, the grating periods are $\bigwedge_{ee} = 15.36\,\mu$m and $\bigwedge_{oo} = 25.30\,\mu$m, respectively, whose signal bandwidths are displayed in Fig. 6b(ii). The bandwidths of the *ee*- and *oo*- processes are 2 nm (red dashed curve) and 33.23 nm (green continuous curve), respectively.

Case – III: $\lambda_p = 777.5$nm:Similarly, for pump, signal, idler at 777.5 nm, 1550 nm, and 1560 nm, respectively, in case of KTP, the grating periods required are $\bigwedge_{ee} = 24.03\,\mu$m and$\bigwedge_{oo} = 6.87\,\mu$m. Figure 6a(iii) shows the calculated signal bandwidths for the two SPDC processes. The bandwidths for the *ee*- and *oo*-processes are 234.23 nm (green continuous curve) and 96.10 nm (red dashed curve), respectively.

In case of LN, with $\bigwedge_{ee} = 18.91\,\mu$m and $\bigwedge_{oo} = 24.00\,\mu$m, the signal bandwidths are 840.84 nm (green continuous curve) and 54.05 nm (red dashed curve), respectively, as shown in Fig. 6b(iii).

Table 2 shows the common overlap bandwidth for a $|\phi^+\rangle$ state, with different input pump wavelengths and for two nonlinear materials. The von Neumann entropy in this case is given as

$$S = -\frac{C_{ee}^2}{C_{ee}^2 + C_{oo}^2}\log_2\frac{C_{ee}^2}{C_{ee}^2 + C_{oo}^2} - \frac{C_{oo}^2}{C_{oo}^2 + C_{ee}^2}\log_2\frac{C_{oo}^2}{C_{oo}^2 + C_{ee}^2} \tag{16}$$

To generate a maximally polarization-entangled state defined in Eq. (12), we require the corresponding ratio of the overlap integrals and the effective indices of the fields involved should be the same, such that the C coefficients are equal. Figure 7a and b shows the variation of S using Eq. (16) in KTP and LN, respectively. It is noticed that the entropy values are close to unity in both cases, showing maximal entanglement of the photons in the polarization state.

Table 2 Common bandwidth for $|\phi^+\rangle$ state compared for three different input pump wavelengths in two nonlinear materials

S.N	Pump λ_p (nm)	Signal λ_s (nm)	Idler λ_i (nm)	Common bandwidth for $\|\phi^+\rangle$ state (nm)	
				KTP	LN
1	532	1550	810	0.96	0.44
2	710	1550	1310	4.40	2.00
3	777.5	1550	1560	96.10	54.05

5 Joint spectral amplitude (JSA) analysis

To characterize the frequency correlation properties of the biphotons, we also study their joint spectral amplitude which provide information about the different degrees of freedom of the photon pairs and their quantum correlations. JSA is a product of PEF (pump envelope function) and PMF (phase-matching function) [22]. PEF and PMF signify the conservation of energy and momentum, respectively, in the SPDC process. The square modulus of these functions results in their corresponding intensities, i.e., PEI (pump envelope intensity), PMI (phase-matching intensity) and JSI (joint spectral intensity).

The width of the PEF depends on the pump bandwidth σ_p, while that of the PMF depends on the waveguide length L and type of quasi-phase-matching. In Fig. 8, we analyze JSA in case of KTP, corresponding to a pump wavelength of 532 nm. In particular, Fig. 8a–c pertains to $|\psi^+\rangle$ state, while Fig. 8d–f pertains to $|\phi^+\rangle$ state. Similarly, in Fig. 9, we analyse the same for LN. In Fig. 8a and d, we have plotted the pump envelope intensity (PEI), considered with bandwidths $\sigma_p = 40$ GHz and 150 GHz, respectively. For KTP, in Fig. 8b, we have shown the phase-matching intensities (PMIs) of the two type-II SPDC processes that lead to the $|\psi^+\rangle$ state (in

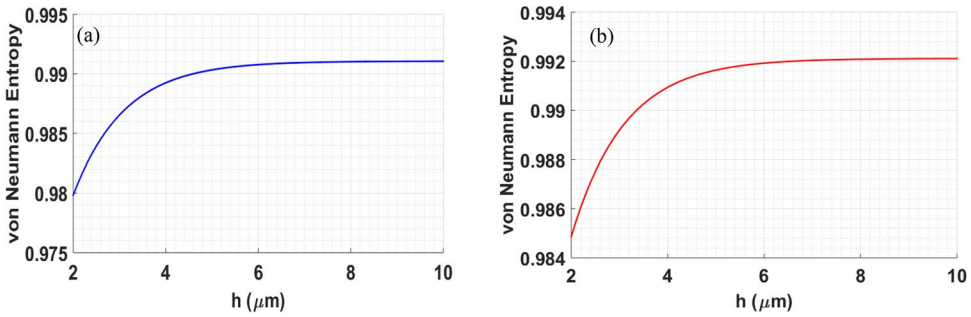

Fig. 7 Variation of von Neumann entropy as a function of the waveguide height (taking width = 6 μm) for the $|\phi^+\rangle$ state in: **a** KTP (blue) and **b** LN (red), corresponding to a pump wavelength of 532 nm

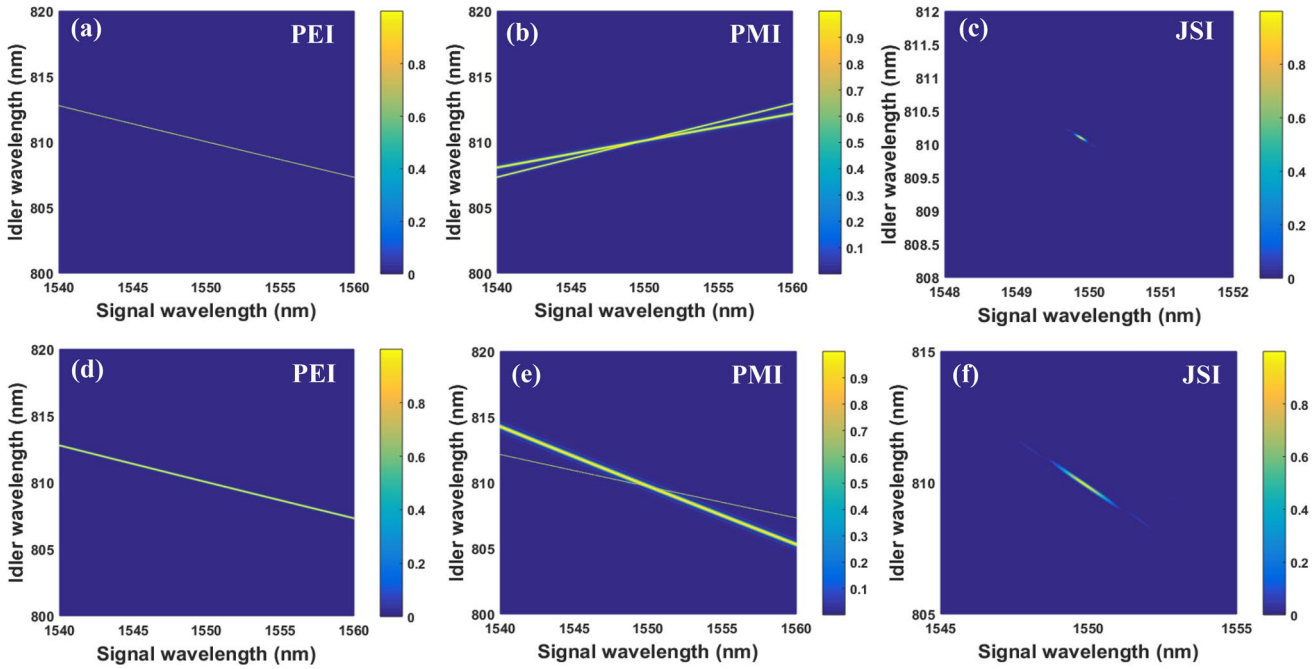

Fig. 8 JSA analysis in KTP for Case–I: $\lambda^p = 532$ nm. **a** PEI with a pulsed pump of bandwidth $\sigma_p = 40$ GHz, **b** PMIs of two type-II PDC processes for $|\psi^+\rangle$ state, **c** overlapped JSIs of two processes involved in $|\psi^+\rangle$ state; **d** PEI with a pulsed pump of bandwidth $\sigma_p = 150$ GHz, **e** PMIs of type-I and type-0 processes for $|\phi^+\rangle$ state, and **f** overlapped JSIs of two processes involved in $|\phi^+\rangle$ state

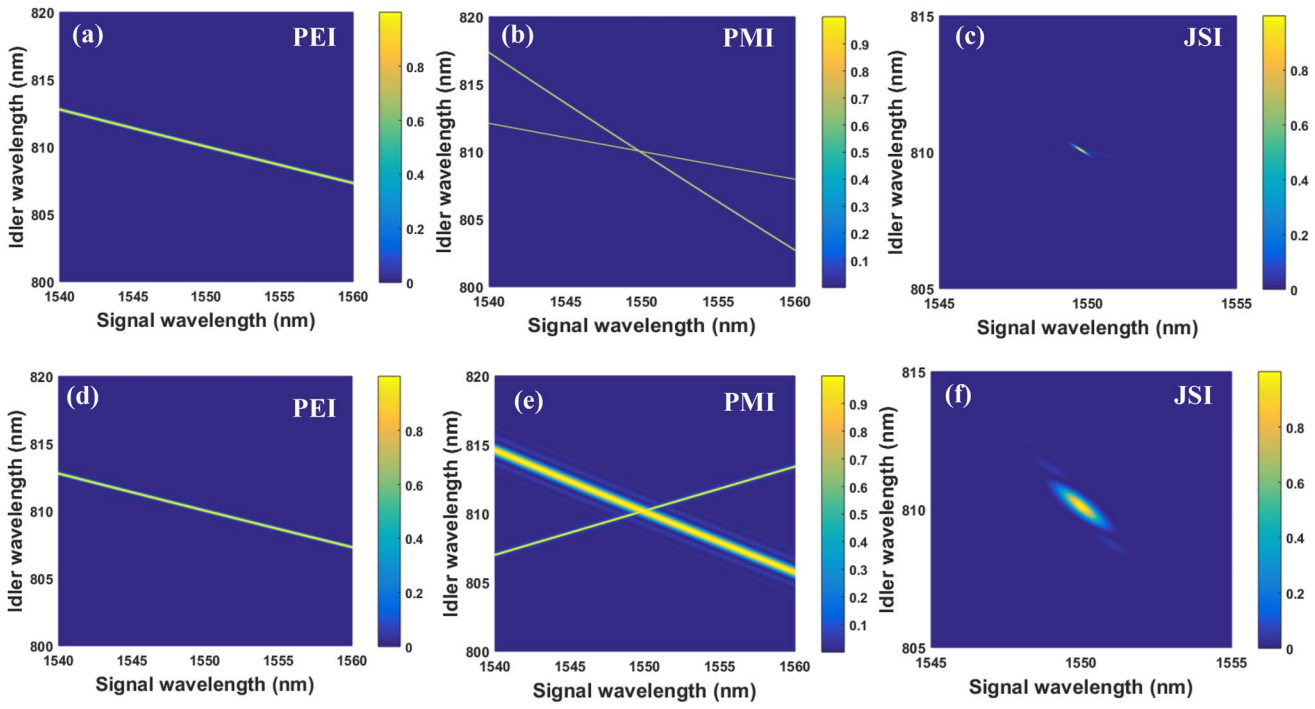

Fig. 9 JSA analysis in LN for Case–I: $\lambda^p = 532$ nm. **a** PEI with pump bandwidth $\sigma_p = 250$ GHz, **b** PMIs of type-II PDC processes for $|\psi^+\rangle$ state, **c** overlapped JSIs of these two processes involved in $|\psi^+\rangle$ state, **d** PEI with pump bandwidth $\sigma_p = 250$ GHz, (e) PMIs of type-I and type-0 process for $|\phi^+\rangle$ state, and **f** overlapped JSIs of two processes involved in $|\phi^+\rangle$ state

Path-I); while in Fig. 8e, we plot PMIs of the type-I (thin curve) and type-0 (thick curve) processes that lead to the $|\phi^+\rangle$ state (in Path-II). The width of a PMI is inversely proportional to the relevant waveguide length, and also depends on the type of quasi-phase-matching, as shown in Fig. 8b and e. Its slope also varies for different phase-matching processes, as shown, due to a difference in the group velocities (of the pump, signal and idler triplet) at different frequencies and polarizations inside the medium [13, 22].

An interesting feature in Fig. 8b is that the two PMI curves cross each other, indicating that in the region of intersection, the signal-idler wavelengths satisfy both the phase-matching conditions pertaining to the two SPDC processes in ppKTP waveguide. And, similarly the same is observed in Fig. 8e. Correspondingly, the overlapping JSIs of these processes are shown in Fig. 8c and f. First, a negative slope of the JSIs indicates the emission of frequency-correlated photon pairs. In addition, overlapping JSIs predict that the photon pairs are entangled.

Thus, from Fig. 8c and f, we infer that the signal/idler photons are in polarization-entangled states $|\psi^+\rangle$ and $|\phi^+\rangle$, respectively. Moreover, the width of the JSI curves indicates the output collection bandwidths in which the signal and idler are entangled, which are different in different cases. We infer that this is far less in case of $|\psi^+\rangle$ as compared to that in case of $|\phi^+\rangle$. Figure 9 depicts the JSA analysis in case of LN. Figure 9a and d shows the pump envelope intensity considered with σ_p= 250 GHz in both cases. In Fig. 9b and e, we have shown the intersecting phase-matching intensities relevant to the$|\psi^+\rangle$, and $|\phi^+\rangle$ states, respectively, in LN. Correspondingly, the overlapping JSIs of these processes are shown in Fig. 9c and f, respectively, signifying entanglement.

6 Conclusion

A common observation for the generation of both entangled states, and irrespective of the material (whether in KTP or in LN), is that with the increase of pump wavelength and especially when the signal and idler wavelengths are similar in values, the common bandwidth enhances, leading to a higher chance of entangled state generation. For example, in case of $|\psi^+\rangle$ state, as we can see in Table 1 and from Fig. 4a(i–iii) for KTP and from Fig. 4b(i–iii) for LN, the common signal bandwidths (relevant for a maximally entangled state) of the two QPM processes, in each case, keep increasing as the signal and idler photons come closer in their wavelengths.

As we compare the generation of two different entangled states, in general for both KTP and LN, we find that the common signal (idler) bandwidths in case of $|\psi^+\rangle$ are far less (detailed in Table 1) compared to that in case of $|\phi^+\rangle$ (detailed in Table 2). Analyzed only for case-1 of these tables, the same is predicted from the JSI widths (of Fig. 8c and Fig. 9c, as compared to that of Fig. 8f and Fig. 9f, wherein the output signal (idler) collection bandwidths are more restrictive in case of $|\psi^+\rangle$ as compared to $|\phi^+\rangle$. However, within the suitable bandwidths, the von Neumann entropy for both the materials is close to unity, which gives a maximally entangled state.

A study of joint spectral amplitude predicts the possibility of frequency correlation of the photon pairs emitted in SPDC, and therefore, the possibility of entanglement in case of biperiod waveguides. The intersection of the PMI curves indicates the possibility of the photon pairs to be entangled. Further, an intelligent choice of the pump parameters and waveguide dimensions, dictates whether the PEI will pass through the region of intersection of the PMIs to result in overlapped JSIs of the two considered SPDC processes, leading to an entangled state. One such case is evident from our JSA analysis in Fig. 8 for KTP. Since the PMIs have a positive slope as in Fig. 8b, only a small pump bandwidth ($\sigma_p = 40$ GHz) could be considered in the PEI plotted in Fig. 8a to obtain a negative slope of the JSI, depicted in Fig. 8c. However, this was not the case for LN, where the pump bandwidths considered (Fig. 9a) could be quite large ($\sigma_p = 250$ GHz). Thus, LN can offer a wide range of pump widths as compared to KTP.

Another significant point in our paper is to generate$|\psi^+\rangle$ and$|\phi^+\rangle$ polarization-entangled Bell states using different QPMs, and hence, different nonlinear coefficients of a material, we compared and discussed the possibility of biperiodic poling, considering different combinations of poling length in a waveguide. This is done to have the same signal powers in the two necessary QPM processes, required to achieve maximal entanglement. Thus, in the above comparisons, one should remember that the ratio of poling lengths in the biperiod poling considered for $|\phi^+\rangle$ is quite different compared to that considered for $|\psi^+\rangle$ [6]. It is easier to achieve maximally entangled photon pairs in the $|\phi^+\rangle$state in KTP as compared to that in LN. In LN, because of the large difference in the nonlinear coefficients, we noted very different poling lengths required to achieve the same signal power emission, leading to maximal entanglement. In addition, this might cause fabrication difficulties of such devices in LN. KTP on the other hand is more practical for such studies. Thus, it is likely that depending on a particular situation, different media and geometry choices will result in better overall performance. Another point of interest of our work is that, in general, for quantum information applications such as superdense coding and quantum teleportation, there is a demand for generating such polarization-entangled states in a single device.

Acknowledgements The authors thankfully acknowledge the following funding agencies: Department of Science & Technology, Ministry of Science and Technology, India (DST/ICPS/QuEST/Theme-l/ 2019,

Project No. 9), and Defence Research and Development Organisation (DFTM/03/3203/P/07/JATC-P2QP-07/463/D(R&D)).

Data availability The data that support the findings of this study are available from the corresponding author upon reasonable request.

References

1. J.G. Titchener, A.S. Solntsev, A.A. Sukhorukov, Phys. Rev. A **92**, 033819 (2015)
2. P.G. Kwiat, J. Mod. Opt. **44**, 2173 (1997)
3. A. Anwar, C. Perumangatt, F. Steinlechner, T. Jennewein, A. Ling, Rev. Sci. Instrum. **92**, 041101 (2021)
4. A. Valles, M. Hendrych, J. Svozilk, R. Machulka, P. Abolghasem, D. Kang, B.J. Bijlani, A.S. Helmy, J.P. Torres, Opt. Express **21**, 10841 (2013)
5. J. Kawashima, M. Fujimura, T. Suhara, I.E.E.E. Photon, Technol. Lett. **21**, 566 (2009)
6. V.K. Shukla, J. Ghosh, Phys. Rev. A **101**, 023832 (2020)
7. K. Thyagarajan, J. Lugani, S. Ghosh, Phys. Rev. A **80**, 052321 (2009)
8. A. Martin, V. Cristofori, P. Aboussouan, H. Herrmann, W. Sohler, D.B. Ostrowsky, O. Alibart, S. Tanzilli, Opt. Express **17**, 1033 (2009)
9. T. Suhara, G. Nakaya, J. Kawashima, M. Fujimura, IEEE Photon Technol. Lett. **21**, 1096 (2009)
10. S. Arahira, N. Namekata, T. Kishimoto, H. Yaegashi, S. Inoue, Opt. Express **19**, 16032 (2011)
11. H. Terashima, S. Kobayashi, T. Tsubakiyama, K. Sanaka, Sci. Rep. **8**, 15733 (2018)
12. R. Kumar, J. Ghosh, Appl. Phys. B **126**, 186 (2020)
13. R. Kumar, J. Ghosh, J. Opt. **20**, 075202 (2018)
14. G.Y. Chen, Z.X. Li, Y.H. Chen, X.D. Zhang, Opt. Express **29**, 12110 (2021)
15. E. Meyer-Scott, N. Prasannan, C. Eigner, V. Quiring, J.M. Donohue, S. Barkhofen, C. Silberhorn, Opt. Express **26**, 32475 (2018)
16. H. Chen, S. Auchter, M. Prilmüller, A. Schlager, T. Kauten, K. Laiho, B. Pressl, H. Suchomel, M. Kamp, S. Höfling, C. Schneider, G. Weihs, APL Photon. **3**, 0804 (2018)
17. J. Lugani, S. Ghosh, K. Thyagarajan, J. Opt. Soc. Am. B **30**, 795 (2013)
18. R. Kumar, V.K. Yadav, J. Ghosh, Phys. Rev. A **102**, 033722 (2020)
19. C. Lanzano, P. Svihra, M. Flament, A. Hardy, G. Cui, A. Nomerotski, E. Figueroa, Sci. Rep. **10**, 6181 (2020)
20. H. Defienne, B. Ndagano, A. Lyons, D. Faccio, Nat. Phys. **17**, 591 (2021)
21. K. Kato and E. Takaoka, Appl. Opt. **41**, 5040–5044 (2002); D. E. Zelmon, D. L. Small, and D. Jundt, J. Opt. Soc. Am. B **14**, 3319–3322 (1997)
22. A. Christ, K. Laiho, A. Eckstein, T. Lauckner, P.J. Mosley, C. Silberhorn, Phys. Rev. A **80**, 033829 (2009)
23. M.A. Nielson, I.L. Chuang, *Quantum Computation and Quantum Information* (Cambridge University, Cambridge, 2006)